Tellus (2001), 53A, 447–468
Printed in UK. All rights reserved

Copyright © Munksgaard, 2001
TELLUS
ISSN 0280–6495

Three-dimensional variational data assimilation for a limited area model

Part II: Observation handling and assimilation experiments

By M. LINDSKOG[1,*], N. GUSTAFSSON[1], B. NAVASCUÉS[2], K. S. MOGENSEN[3], X.-Y. HUANG[3], X. YANG[3], U. ANDRÆ[1], L. BERRE[1,4], S. THORSTEINSSON[1,5] and J. RANTAKOKKO[6], [1]*Swedish Meteorological and Hydrological Institute, S-60176 Norrköping, Sweden;* [2]*National Meteorological Institute of Spain, Madrid, Spain;* [3]*Danish Meteorological Institute, Copenhagen, Denmark;* [4]*Météo-France, Toulouse, France;* [5]*Icelandic Meteorological Office, Reykjavik, Iceland;* [6]*Uppsala University, Uppsala, Sweden*

(Manuscript received 17 March 2000; in final form 6 February 2001)

ABSTRACT

A 3-dimensional variational data assimilation (3D-Var) scheme for the HIgh Resolution Limited Area Model (HIRLAM) forecasting system is described. The HIRLAM 3D-Var is based on the minimisation of a cost function that consists of one term, J_b, which measures the distance between the resulting analysis and a background field, in general a short-range forecast, and another term, J_o, which measures the distance between the analysis and the observations. This paper is concerned with J_o and the handling of observations, while the companion paper by Gustafsson et al. (2001) is concerned with the general 3D-Var formulation and with the J_b term. Individual system components, such as the screening of observations and the observation operators, and other issues, such as the parallelisation strategy for the computer code, are described. The functionality of the observation quality control is investigated and the 3D-Var system is validated through data assimilation and forecast experiments. Results from assimilation and forecast experiments indicate that the 3D-Var assimilation system performs significantly better than two currently used HIRLAM systems, which are based on statistical interpolation. The use of all significant level data from multilevel observation reports is shown to be one factor contributing to the superiority of the 3D-Var system. Other contributing factors are most probably the formulation of the analysis as a single global problem, the use of non-separable structure functions and the variational quality control, which accounts for non-Gaussian observation errors.

1. Introduction

The aim of this paper is to give a description of the treatment of observations in the HIRLAM 3D-Var. In addition, results from parallel data assimilation and forecast experiments are described. In the parallel experiments the performance of the 3D-Var scheme is compared with data assimilation based on statistical interpolation (or OI, Optimum Interpolation) of observed deviations from a short range forecast (Lorenc, 1981). The general formulation of the HIRLAM 3D-Var and the treatment of the background field are the subjects of a companion paper by Gustafsson et al. (2001).

All observation values to be used in the HIRLAM 3D-Var are subject to data screening with the main emphasis on rejecting crude observation errors and on removing redundant informa-

* Corresponding author.
e-mail: magnus.lindskog@smhi.se

tion. In addition, the observation error constraint J_o has been modified to include a variational quality control (Andersson and Järvinen, 1999). This variational quality control is based on a maximum likelihood formulation, where observation errors are assumed to consist of a gross error, with a rectangular probability distribution, in addition to an error with a Gaussian probability distribution.

The observation handling, with emphasis on observation screening, is described in Section 2 of this paper together with a brief discussion on the parallelisation of the computer code. The observation operators (i.e., the J_o formulation and the variational quality control) are the subject of Section 3. Results from the parallel data assimilation and forecast experiments are given in Section 4. The effects of using all significant level data from multilevel observation reports are examined in Section 5, followed by an investigation of the functionality of the observation quality control in Section 6. A discussion and some concluding remarks are presented in Section 7.

2. The observation handling system

2.1. Data handling

Due to increased data volumes, new data types and more advanced computer architectures an advanced data handling system is required. An overview of the system is given in Fig. 1. Observations (y) in binary universal form for the representation of meteorological data (BUFR) are processed and an observation data file in the central memory array (CMA) format, which is designed to be suitable for use in variational data assimilation, is prepared. While the CMA is being prepared, necessary information is crudely checked and, if necessary, observed variables are transformed into those used directly by the variational assimilation. Observation error standard deviations are assigned during this step. The main functions of the screening are quality control using various algorithms, including a comparison with the background field, data rejections and data thinning to select only those observed values that actually will be used by the variational data assimilation. The HIRLAM 3D-Var produces the analysis (x) file and a CMA file updated with information, such as the deviations between the observations and the analysis in the positions of the observations. During the feedback of observations the updated CMA file is read and information added by the HIRLAM 3D-Var is inserted into the original observation data file in BUFR format. Finally, the updated data are read and various diagnostics, needed for validation of the performance of the variational data assimilation, are produced.

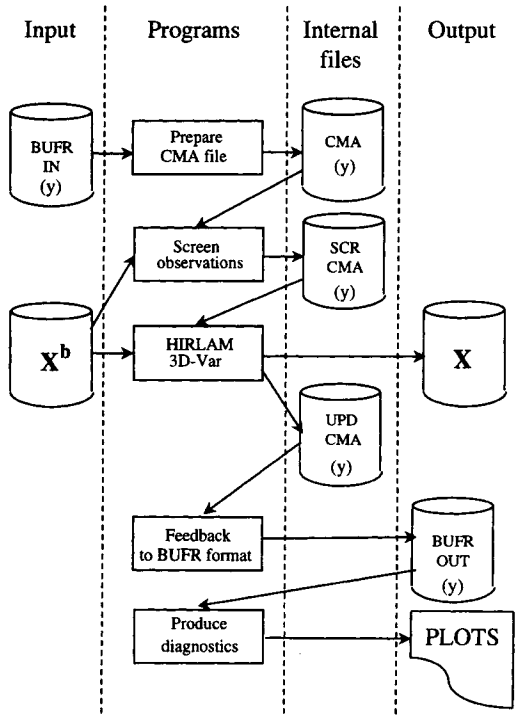

Fig. 1. Overview of the main modules (boxes) and files (barrels) in the observation handling system.

Parts of the software package for observation handling, including the programs for preparing the CMA and feeding information back to the original observation data file, are shared with the European Centre for Medium-Range Weather Forecasts (ECMWF).

2.2. Screening

Observations are rejected by the screening for several reasons. Some of the screening algorithms are simple logical checks verifying that observations are situated within the analysis area and that SHIP reports originate from ocean areas.

There are also representativity checks; for example stations situated too far away from the model orography are rejected. The most important check is the first guess check, to be described in more detail below. The blacklisting, finally, makes it possible to reject observations that are coming from stations situated in particular geographical areas or observations that come from particular stations that are considered to be of poor quality.

After the individual screening checks, a sequence of combination checks is carried out. A multilevel check is applied to multilevel report data. If more than four consecutive levels are flagged as suspicious by the screening, all of these data are rejected. For land surface stations the observed station altitude pressure and the corresponding geopotential height are selected rather than the mean sea level pressure and the corresponding zero height. Finally, a data redundancy check is applied. All land surface observations located at the same horizontal position that have passed the former tests are compared. Only the observation closest to the time of analysis is accepted. Radiosondes and PILOT balloon reports are simultaneously checked. If both types of reports exist from the same station the radiosonde report is selected by preference. Furthermore, in the case of multiple reports of the same type, the one closest to analysis time is chosen. For the moving platforms, a thinning is applied. The minimum horizontal distance allowed between observations from the same station identifier has initially been set to half a grid distance. For observations from the same station identifier closer than half a grid distance, only the observation closest to the time of the analysis is retained. For aircraft observations, however, the thinning is not applied if the vertical pressure difference exceeds 50 hPa.

In the first guess check the background model state $\boldsymbol{x}^{\mathrm{b}}$ is projected on the observed quantity y_i with the observation operator H (see Subsection 3.1). The squared background departure from the observation i is calculated and normalised with the sum of the observation error variance, $\sigma^2_{\mathrm{o},i}$, and the background error variance, $\sigma^2_{\mathrm{b},i}$. The observation, y_i, is rejected if it does not satisfy the following inequality:

$$L_1 \leqslant ([H(\boldsymbol{x}^{\mathrm{b}})]_i - y_i)|([H(\boldsymbol{x}^{\mathrm{b}})]_i - y_i)|/(\sigma^2_{\mathrm{b},i} + \sigma^2_{\mathrm{o},i}) \leqslant L_2, \quad (1)$$

where L_1 and L_2 are the upper and lower rejection limits and $[H(\boldsymbol{x}^{\mathrm{b}})]_i$ denotes the projection of the model state on observation i. The rejection limits currently used are obtained from historical rejection series of the OI system, and are dependent on type of variable. Since satellite cloud track wind (SATOB) observations are systematically too weak, $-L_1$ is smaller than L_2 for this particular observation type. For all other data $-L_1$ is equal to L_2. The coefficients L_1 and L_2 will later on be re-tuned, based on rejection series from the 3D-Var system.

In the case of wind, both components are checked jointly. For high level winds with wind speed greater than 15 m/s, a wind direction check is applied.

Spatially varying first guess error standard deviations are used to represent the differences in background error statistics resulting from different flow characteristics in different geographical areas, as well as from variations in the station density. These standard deviations have been estimated for data from the observation types presented in Subsection 3.2 by applying the NMC method (Parrish and Derber, 1992) to 3 months of ECMWF +24 and +48 h forecasts. ECMWF forecasts were chosen in order to obtain a global coverage, which is desired since HIRLAM countries apply the assimilation system over different geographical areas, having different spatial background error distributions. A total of 15 standard pressure levels were used in the vertical together with a low horizontal resolution ($5^\circ \times 5^\circ$) grid, in order to avoid noisy variances. The representativeness of the ECMWF statistics with respect to the HIRLAM model errors was verified by comparing the ECMWF statistics with HIRLAM statistics, obtained with the NMC method over a limited area.

2.3. *Parallelisation*

The calculations in the screening and the HIRLAM 3D-Var require that all observations are kept in the computer memory simultaneously. The observation handling includes a calculation work load that is irregular in space as well as in time due to the spatial and temporal distributions of the observations. The calculation work load for the observation operators is dominated by calculations in data-dense areas like continental North

America, continental Europe, and along satellite tracks. In order to achieve an even work load distribution among the processors of a parallel computer, a parallelisation strategy that takes the actual observation distribution into account is applied.

The parallelisation of the J_b grid point space calculations, as well as the corresponding spectral model calculations, builds on a sub-division of the model domain into equally sized sub-areas and a distribution of one such sub-area to each processor of the parallel computer. The main parallelisation strategy, as proposed by Rantakokko (1997), for the treatment of observations in the HIRLAM 3D-Var is a combination of the following two extreme strategies:

(A) Distribute all the observations in accordance with the horizontal position of the observations to the processors on which the corresponding sub-area of the grid point fields resides. Carry out all the observation operator calculations on the same processor.

(B) Distribute the observations, independent of their horizontal positions, to the available processors in such a way that each processor will have the same amount of computational work for the observation operators. One possibility is to distribute an equal number of observations of each type to each processor. Fetch the grid point values needed for observation operator calculations by message passing.

Strategy A is simple and identical to the parallelisation of the forecast models. The disadvantage is a poor load balance of the observation operator calculations. Strategy B has a good load balance in the observation operator calculations, the disadvantage being the need to communicate grid point information between the processors; the efficiency of this may depend on the speed of the communication network between the processors. For the HIRLAM 3D-Var the horizontal interpolation part of the observation operator is carried out in accordance with strategy A, and the remaining parts of the observation operator calculations are carried out in accordance with strategy B. This "main" parallelisation strategy is memory consuming, since the horizontally interpolated grid point fields need to be calculated in advance and stored in the computer memory for all observation positions. Therefore the parallelisation strategy A is available as an option, for computers with too small memory for the main strategy.

The parallelisation of the HIRLAM variational data assimilation is based on explicit message passing, i.e., intermediate calculation results are communicated between the computer processors by means of messages.

3. The observation error constraint

The observation error constraint J_o measures the distance between the model state $\boldsymbol{x}$ and the observations $\boldsymbol{y}$. The observation operator H provides a link between the model state vector $\boldsymbol{x}$ and the observation vector $\boldsymbol{y}$ through the model equivalent of the observed quantities $H\boldsymbol{x}$ at the positions of the observations. The observation operator H may be (weakly) non-linear. This non-linearity may be important to utilize, for example with regard to the connection between model temperature and humidity profiles and radiances at the top of the atmosphere to be compared with measured satellite radiances. Also for conventional observations, for example temperatures and winds observed with pressure as the vertical coordinate, the observation operator is weakly non-linear since the pressures of the model levels depend on the model state variable surface pressure.

We have chosen to simplify the vertical interpolation part of the observation operator by applying the full non-linear vertical interpolation to the background field $\boldsymbol{x}^b$, while the tangent-linear vertical interpolation is applied to the analysis increment $\delta\boldsymbol{x} = \boldsymbol{x} - \boldsymbol{x}^b$. The linearisation is carried out with reference to the background field $\boldsymbol{x}^b$. We have also chosen to carry out the tangent-linear approximation for the other parts of the observation operator, for example calculation of geopotential heights at model levels and extrapolation of geopotential height below the model orography. This means that the observation error constraint may be written as follows:

$$J_o = \tfrac{1}{2}(H\boldsymbol{x}^b + \boldsymbol{H}\delta\boldsymbol{x} - \boldsymbol{y})^T \boldsymbol{R}^{-1}(H\boldsymbol{x}^b + \boldsymbol{H}\delta\boldsymbol{x} - \boldsymbol{y}), \tag{2}$$

where $\boldsymbol{H}$ denotes the tangent-linear observation operator, linearised around the background field $\boldsymbol{x}^b$. Since $\boldsymbol{H}$ is linear, the gradient of the observation error constraint J_o with regard to the model

state increment vector $\delta \boldsymbol{x}$ is readily obtained:

$$\nabla_{\delta x} J_o = (\boldsymbol{H})^T \boldsymbol{R}^{-1}(H\boldsymbol{x}^b + \boldsymbol{H}\delta\boldsymbol{x} - \boldsymbol{y}). \quad (3)$$

The observation errors are assumed to be un-correlated. This is considered to be appropriate with regard to the current scheme for selection of observations. With this assumption, the covariance matrix $\boldsymbol{R}$ for the observation errors becomes a diagonal matrix and only the observation error standard deviations need to be specified. To account for non-Gaussian observation errors a variational quality control is applied (see Subsection 3.3).

3.1. *The observation operators*

The observation operator H and the tangent-linear observation operator $\boldsymbol{H}$ are sub-divided into a sequence of sub-operators. Formally, we may write:

$$H = H_{spec} I_v P_{calc} \boldsymbol{I}_h \boldsymbol{F}^{-1}, \quad (4)$$

where $\boldsymbol{F}^{-1}$ is an inverse Fourier transform, $\boldsymbol{I}_h$ denotes horizontal interpolation of model level data from grid points to the horizontal positions of the observations, P_{calc} calculation of pressures and geopotentials at model full and half levels, I_v vertical interpolation to the levels of the observed data values and H_{spec} any other specialised operators for each type of observation. The inverse Fourier transform is described in the companion paper by Gustafsson et al. (2001) and for the non-linear observation operator, H, it will only be applied in the case of a spectral forecast model.

The background field $\boldsymbol{x}^b$ as well as the increment field $\delta \boldsymbol{x}$ at the positions of the observations are calculated by bi-linear horizontal interpolation.

Starting from model state variables interpolated to the observation positions, the pressures at the model levels are calculated according to the definition of pressure at model full and half levels. Geopotentials at model half levels are obtained by integration of the hydrostatic equation. For the treatment of PILOT wind reports, reporting at height levels, the model full level geopotentials are also needed. These are obtained by a simple linear vertical interpolation, with respect to the logarithm of the pressure, from the model half level geopotentials.

The vertical interpolation of model background fields from model levels to observation levels is in general carried out linearly in logarithm of pressure. For PILOT wind observations reporting at height levels, the vertical interpolation is carried out linearly with the geopotential as the vertical coordinate.

With regard to the conventional observations, only a few special types of sub-operators are applied at present: the extrapolation of geopotential below the model lower boundary surface and the calculation of wind, temperature and humidity at the reporting levels of SYNOP, SHIP and DRIBU reports.

Geleyn (1988) describes a method to calculate the vertical interpolation between the lowest model level and the surface. We use this method to interpolate model values for the observed 10 m wind (u_{10m}, v_{10m}) as well as the 2 m temperature (T_{2m}) and relative humidity (RH_{2m}) from SYNOP, SHIP and DRIBU reports. This highly non-linear operator based on the Monin-Obukhov similarity theory for the surface layer takes turbulence and terrain characteristics into account. The following two modifications of the method introduced by Geleyn (1988) are made. The roughness length over open sea is iteratively determined from the surface friction velocity (u^* in the Charnock formula). In addition, the formula is improved with an additional term dependent on "gustiness stability", to ensure that in low wind and unstable conditions the heat fluxes do not drop to zero because of a vanishing roughness.

Taking into account that the horizontal interpolation and the inverse Fourier transform are linear, the tangent-linear observation operator may formally be written as follows:

$$\boldsymbol{H} = H' = (H_{spec})'(I_v)'(P_{calc})' \boldsymbol{I}_h \boldsymbol{F}^{-1}, \quad (5)$$

where $(H_{spec})'$ and $(P_{calc})'$ are the tangent-linear versions of H_{spec} and P_{calc}, respectively. Here $(I_v)'$ denotes a simplified tangent-linear version of I_v. It has been developed to make the calculations more efficient by ignoring the surface pressure increment dependencies in the vertical interpolation of temperature, wind and specific humidity.

3.2. *Data usage and observation errors*

Important features of the variational data assimilation are the global usage of data, i.e., all data in the model domain are used at once to solve a single global problem (Parrish and Derber, 1992),

and the rational use of observations that are non-linearly coupled to the forecast model variables (Gustafsson et al., 1997). The latter potential advantage is not yet fully realised in the present version of the HIRLAM 3D-Var system, in which the following observed values are utilised.

- For TEMP reports, all significant level data of temperature, wind and specific humidity are utilised.
- For SYNOP, SHIP and DRIBU reports, the station level height, multiplied by the gravitational acceleration, g, is utilised as a geopotential observation at the observed station level pressure. The observed 10 m wind (u_{10m}, v_{10m}) as well as 2 m temperature (T_{2m}) and relative humidity (RH_{2m}) may also be utilised. At present only 10 m winds from SHIP reports are used.
- For AIREP reports, wind and temperature observations are utilised.
- For PILOT wind reports, all significant level wind data, observed at pressure or height levels, are utilised.
- For SATOB reports, wind observations are utilised.

The standard deviations of observation errors utilised in the HIRLAM 3D-Var were originally obtained from the ECMWF 3D-Var (Courtier et al., 1998). These were based on statistical evaluation of observing systems over long periods. An examination of the amplitude of the innovation vectors (which are departures between +6 h forecasts and observations) and a comparison with error statistics applied at the United Kingdom Meteorological Office (Parrett, 1992) led to a revision of the original observation error standard deviations. The resulting observation error standard deviations are presented in Table 1 for upper air observation types and in Table 2 for surface observation types. The observation errors include both instrumental and representativeness errors. For continuity reasons the standard deviations are interpolated in the logarithm of the pressure to the observed pressure. Above 10 hPa and below 1000 hPa the errors are assumed constant.

An empirical regression relation is used to specify the relative humidity observation error standard deviations, σ_o. The relation, which is obtained through a statistical analysis of the dependence of the errors on temperature, yields:

$$\sigma_o = -0.0015T + 0.54 \quad \text{for } 240\ \text{K} < T < 320\ \text{K}. \tag{6}$$

For temperatures below 240 K, σ_o takes the value 0.18 and for temperatures above 320 K it takes the value 0.06. The observation error standard deviation for specific humidity is derived from the tangent-linear relationship that relates specific and relative humidities.

Table 1. *Observation error standard deviations for upper air data*

Pressure (hPa)	TEMP u/v (m/s)	SATOB u/v (m/s)	AIREP u/v (m/s)	PILOT u/v (m/s)	TEMP T (K)	AIREP T (K)
1000	2.1	2.0	2.5	2.3	1.1	1.4
850	2.0	2.0	2.5	2.3	0.9	1.3
700	2.0	2.0	3.0	2.5	0.8	1.2
500	2.5	3.5	3.5	3.0	0.8	1.2
400	3.1	4.3	4.0	3.5	0.8	1.2
300	3.6	5.0	4.0	3.7	1.0	1.3
250	3.8	5.0	4.0	3.5	1.1	1.3
200	3.5	5.0	4.0	3.5	1.1	1.4
150	3.1	5.0	4.0	3.4	1.1	1.4
100	2.9	5.0	4.0	3.3	1.0	1.4
70	2.5	5.0	4.0	3.2	0.9	1.5
50	2.3	5.0	4.0	3.2	1.0	1.6
30	2.3	5.0	4.0	3.3	1.1	1.8
20	2.2	5.0	4.0	3.6	1.1	2.0
10	2.2	5.7	4.0	4.5	1.1	2.2

Table 2. *Observation error standard deviations for surface data*

Pressure (hPa)	DRIBU Z (m)	SYNOP Z (m)	SHIP Z (m)	DRIBU u/v (m/s)	SYNOP u/v (m/s)	SHIP u/v (m/s)	DRIBU T (K)	SYNOP T (K)	SHIP T (K)
1000	11.5	7.0	14.0	2.4	3.0	3.0	1.8	2.0	1.8
850		8.0			3.0			1.5	
700		8.6			3.0			1.3	
500		12.1			3.4			1.2	
400		14.9			3.6			1.3	
300		18.8			3.8			1.5	

3.3. *Variational quality control*

The variational assimilation algorithm is formulated on the basis of Bayes theorem (Lorenc, 1986), identifying the cost function J with the logarithm of a probability density function (p.d.f.). The variational quality control (VarQC) accounts for the possibility of gross errors, represented by a flat p.d.f., in the data presented to the variational analysis (Lorenc and Hammon, 1988; Ingleby and Lorenc, 1993; Andersson and Järvinen, 1999), in addition to random errors, represented by a Gaussian p.d.f.. For an individual observation value, y_i, given the state vector $\boldsymbol{x}$, the p.d.f. is given by:

$$p_i = P\frac{1}{D} + (1-P)\frac{1}{\sqrt{2\pi}\sigma_i}\mathrm{e}^{(-0.5z_i^2)}, \tag{7}$$

where P stands for the a priori probability of observation i having a gross error.

$$z_i = \frac{y_i - [H\boldsymbol{x}]_i}{\sigma_i}$$

is the departure between the observed value, y_i, and the model state projected on observation i, normalised by the observation error standard deviation (σ_i). The factor D represents the range of possible values, all with the same probability in the case of gross error. It is assumed that the data presented to the variational analysis have been previously checked, in order to keep the absolute value of z_i less than $D/(2\sigma_i)$ (D needs to be consistent with the parameters L_1 and L_2 mentioned in Subsection 2.2). The effect of the VarQC is to scale the magnitude of the gradient of the observation part of the cost function obtained assuming a Gaussian error distribution only. An observation is considered rejected when the following scaling factor, or the a posteriori weight, r, is less than 0.75:

$$r = \frac{\nabla_{z_i} J_{\mathrm{o},i}^{\mathrm{QC}}}{\nabla_{z_i} J_{\mathrm{o},i}}, \tag{8}$$

where $J_{\mathrm{o},i}^{\mathrm{QC}}$ and $J_{\mathrm{o},i}$ are the contributions from observation i to the observation part of the cost function with and without VarQC, respectively. These are given by identifying the observation part of the cost function with the logarithm of p_i according to (7), with P larger than zero and equal to zero, respectively. The value of r depends on the a priori parameters P and D as well as on the normalised departure z_i. Following the procedure used at ECMWF (Andersson and Järvinen, 1999) for this purpose, P and D have been estimated from the historical rejections series of operational HIRLAM OI analyses, for the different variables of all kind of observation reports. The values obtained clearly show a dependence on observation system and variable, as well as on observation density. The latter dependence has not yet been taken into account in the HIRLAM 3D-Var.

For wind data, it is assumed that gross errors affect both of the wind components and these are checked jointly.

Because of the global data usage in 3D-Var, all observations are used in VarQC to support or reject an observation. Due to the iterative nature of the variational procedure, the a posteriori weight, r, evolves with the number of cost function evaluations. Observations are not definitively rejected or accepted at a fixed calculation step. At present, since a spatially varying P has not yet been introduced, there is no direct dependence on the first guess error or the analysis error. However, we have chosen to switch on the VarQC only after a number of iterations has been performed (20 in

the assimilation experiments presented here). One iteration consists of one or more cost function evaluations. In our assimilation experiments 70 iterations in general corresponded to roughly 75 cost function evaluations. This prevents the rejection of observations located in poor first guess zones, by allowing the initial guess (i.e., the initial field when the VarQC is switched on) to be closer to observations than the first guess. It may furthermore be added that the cost function including VarQC is not strictly quadratic and relative minima may occur. The final analysis therefore depends on the starting initial guess and it may be beneficial to have an improved initial guess before adding this non-quadratic feature of the cost function. Furthermore, after a number of iterations (70 in the assimilation experiments presented here) the VarQC is again switched off. To improve the convergence the last cost function evaluations are performed only with observations accepted in the VarQC.

It should be added that, although the use of VarQC implies a non-quadratic cost function, it has a smoothing effect on the minimisation. If two observations that are not fully consistent with each other are presented to the minimisation problem, an oscillation between two very distinct solutions may occur at different cost function evaluation steps. Since VarQC reduces the weights given to less consistent observations, these oscillations are reduced and the two originally very distinct solutions converge.

4. Assimilation experiments

Two sets of assimilation experiments, using different versions of the HIRLAM system, were performed over an area covering Northern Europe and the Northern Atlantic to evaluate the performance of the variational data assimilation. One experiment was for a late summer period and another for a winter period. The summer experiment extended from 25 August to 24 September 1995 and the winter experiment from 10 February 1998 to 9 March 1998. Both of these periods were characterised by several cyclones passing over the Northern Atlantic and through the Baltic Sea area.

The two sets of assimilation experiments consist of runs with three different combinations of analysis and forecast model formulations: (1) OI analysis together with the HIRLAM grid point forecast model; (2) 3D-Var analysis with the HIRLAM grid point forecast model; (3) 3D-Var analysis with the HIRLAM spectral forecast model.

The main reason for using these three different experimental combinations is that the OI based HIRLAM system, currently used operationally by several weather services, includes the grid point forecast model, while the HIRLAM 3D-Var was developed from the spectral version of the HIRLAM forecast model (Gustafsson, 1999; Gustafsson et al., 2001). Thus, in the experiments, both the grid point and the spectral models were used together with the 3D-Var.

For each of the configurations described above, data was assimilated in a 6 h assimilation cycle. The observations were retrieved from the ECMWF archive. After each analysis, a non-linear normal mode initialisation was applied (Machenhauer, 1977), followed by a +48 h forecast. For the lateral boundary conditions, 6-hourly ECMWF analyses were used.

The parallel experiments for the summer period were conducted on a Fujitsu VPP700 vector computer at ECMWF using a single processor. The model grid mesh consisted of 162×142 horizontal grid points at 0.5° resolution, and 31 vertical levels. The winter case experiments were run on a CRAY T3E parallel computer using 36 processors; 202×178 horizontal grid points with a resolution of 0.4° and 31 vertical levels were used for these runs.

The spectral and grid point forecast models used for the summer case experiments were based on the current HIRLAM reference forecast model physics (version 4.3, 1999), while the spectral and grid point forecast models used for the winter case were based on the forecast model physics used operationally at SMHI (version 2.7.15, 1999). The main differences between these physics packages are related to parameterisations of turbulence, clouds and condensation. The HIRLAM reference model physics uses a first-order non-local turbulence closure scheme by Holtslag and Bovine (1993). For the clouds and condensation parameterisation, the STRACO scheme is applied (Sass et al., 1999). The main features of this scheme include sub-grid scale condensation with a statistical distribution of cloud condensate, a smooth transition between stratiform and convective

regimes and microphysics of condensation according to Sundqvist (1993). The operational version at SMHI uses a first order local vertical diffusion scheme (Louis, 1979) and a cloud and condensation scheme based on explicit forecasts of cloud water (Sundqvist et al., 1989). Both the reference and the SMHI models use a radiation scheme based on ideas of Savijärvi (1989).

Eulerian time integration and a fourth order implicit horizontal diffusion scheme were used in all model integrations. The summer case forecasts were run with a 240 s time step and for the grid point formulation the horizontal diffusion coefficient in the troposphere was set to 3.5×10^{14} m^4/s, while for the spectral formulation it was set to 1.75×10^{14} m^4/s in the troposphere. The smaller horizontal diffusion coefficients for the spectral model may be motivated by its inherent smoothing due to spectral truncation and by its more complete diffusion operator. Based on earlier experiences, a slight increase in the coefficient was introduced in the stratosphere, for both forecast model formulations and for both the summer case and the winter case. The winter case experiments with the grid point formulation of the forecast model were run with a 120 s time step and the horizontal diffusion coefficient set to 1.5×10^{14} m^4/s. Due to the filtering effect of the spectral truncation it was possible to increase the time step used for the spectral forecast model to 200 s. For the spectral model the horizontal diffusion coefficient was set to 3.0×10^{13} m^4/s.

For the winter case OI and 3D-Var assimilation experiments, only conventional types of observations were assimilated. These included SYNOP, SHIP, DRIBU, AIREP, PILOT and TEMP observation reports. For the summer case experiments satellite cloud track wind (SATOB) observations were also used in both the OI and 3D-Var system. A few differences between data usage in the OI and 3D-Var systems should be pointed out: (1) Wind observations from DRIBU reports and SYNOP coastal station reports are used only by OI, whereas temperature observations from AIREP reports are used only by 3D-Var. (2) The 3D-Var system assimilates TEMP and PILOT winds, as well as TEMP temperatures and moisture, from all significant levels, whereas the OI system assimilates TEMP and PILOT winds, as well as TEMP geopotential heights and moisture, at standard pressure levels only, in addition to geopotential height at the observed surface pressure. (3) The 3D-Var system assimilates specific humidity whereas the OI system assimilates relative humidity. The minimisation of the cost function of the 3D-Var system was performed until a quadratic norm of the cost function gradient had decreased by a factor 20 as compared with the first gradient evaluation. Further decrease of the norm of the gradient gives very minor reduction in the cost function and very small changes to the assimilation increments. A simple analysis of sea surface temperature (SST) and ice cover, based on the successive correction method, initially introduced by Bergthorsson and Döös (1955), complemented the OI and 3D-Var analyses.

To evaluate the relative quality of the OI and 3D-Var analyses and subsequent forecasts, we verified them against observations in the list of (radiosonde and SYNOP) stations established by the European Working Group on Limited Area Models (EWGLAM). The verification was done for key weather parameters, at the surface level, and at the vertical levels of 850, 500 and 300 hPa. The model data used in the statistics were the analyses and the +6, +12, +18, +24, +30, +36, +42 and +48 h forecasts.

4.1. *Summer period observation verification results*

Fig. 2 illustrates the time-averaged summer period bias and root mean square error (rms) scores for mean sea level pressure (P_{msl}) analyses and forecasts and 2 m temperature (T_{2m}) forecasts, in comparison to the observations. The HIRLAM forecasts tend to have an increasingly larger negative bias in the P_{msl} field with increasing forecast length. However, the bias in P_{msl} forecasts based on 3D-Var analyses are smaller than those with OI analyses. Better performance with 3D-Var based forecasts are also seen in terms of rms values. Among the forecasts initiated with 3D-Var analyses, the spectral model forecasts are seen to be slightly better than those of the grid point model. For T_{2m} all the forecast results showed a trend of gradual warming with increasing forecast length, in particular for the 3D-Var based ones. It seems that the grid point model 3D-Var T_{2m} forecasts are more biased than the spectral model 3D-Var forecasts. The rms scores of the OI T_{2m} forecasts are rather similar to the scores of 3D-Var spectral model forecast, whereas the scores of the

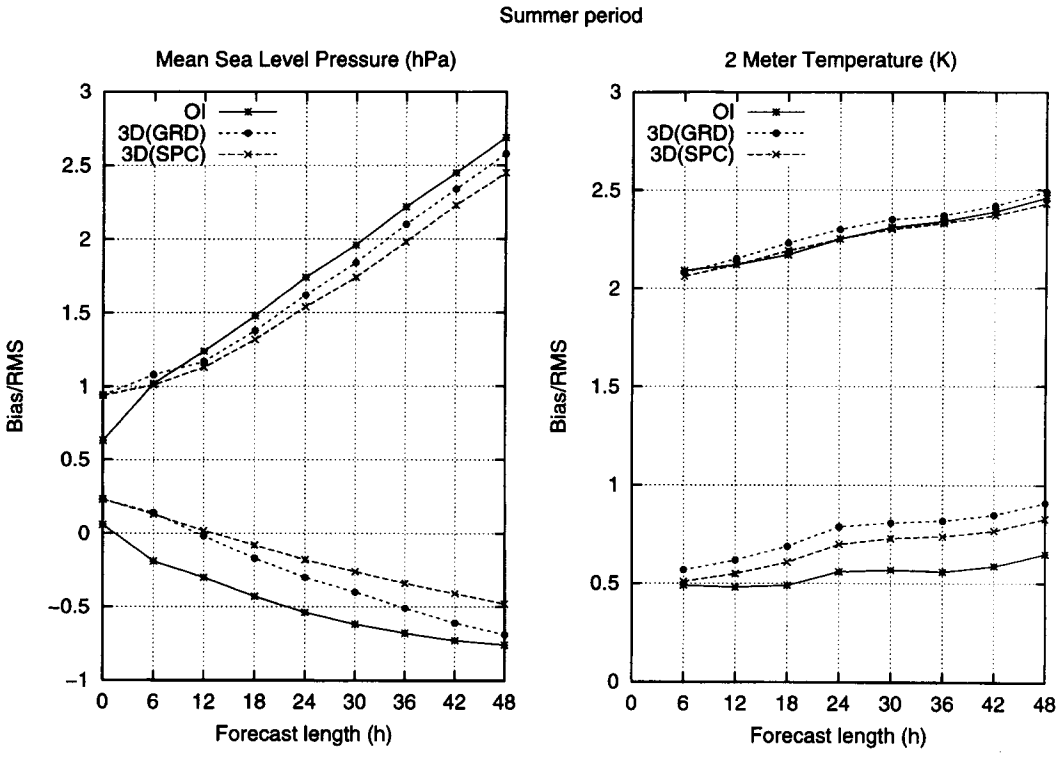

Fig. 2. Average bias and rms scores for summer period (25 August–24 September 1995) P_{msl} (left) and T_{2m} (right) forecasts as functions of forecast length (h). The P_{msl} (hPa) and T_{2m} (m/s) scores are for OI (full), 3D-Var with grid point forecast model (dashed with dots) and 3D-Var with spectral forecast model (dashed with crosses).

3D-Var grid point model forecasts are somewhat worse.

For all the bias and rms scores with various configurations, as described above, large temporal variability in observation verification scores is seen for different model variables. As an example, Fig. 3 shows the bias and rms values of the +24 h P_{msl} forecasts, in comparison to verifying observations, for the entire summer period. Since the variability of the spectral and grid point model forecasts launched from 3D-Var analyses show strong agreement, only the grid point model 3D-Var forecasts and the OI forecasts are shown. The OI and 3D-Var results are seen to outperform each other during different periods, although most often the 3D-Var scores are better.

The time-averaged bias and rms scores for the summer period analyses and forecasts of geopotential height, temperature and wind speed at the 850, 500 and 300 hPa levels are shown in Fig. 4. The better initial time rms scores for the OI geopotential height and for the 3D-Var temperature are consequences of the fact that the OI system assimilates geopotential heights, whereas the 3D-Var system assimilates temperatures. In terms of rms, the scores for the 3D-Var based forecasts are better than the OI forecasts, for all variables and vertical levels, except for the 300 hPa level temperatures, for which the rms scores are rather similar. In general the 3D-Var spectral model forecasts are slightly better than the 3D-Var grid point model forecasts. In terms of bias, the scores of the geopotential height and wind forecasts based on the 3D-Var are better than the scores of the OI based forecasts. Again, the scores of the 3D-Var spectral model forecasts are better than those for the grid point model. For temperatures, the bias of the OI and 3D-Var forecasts

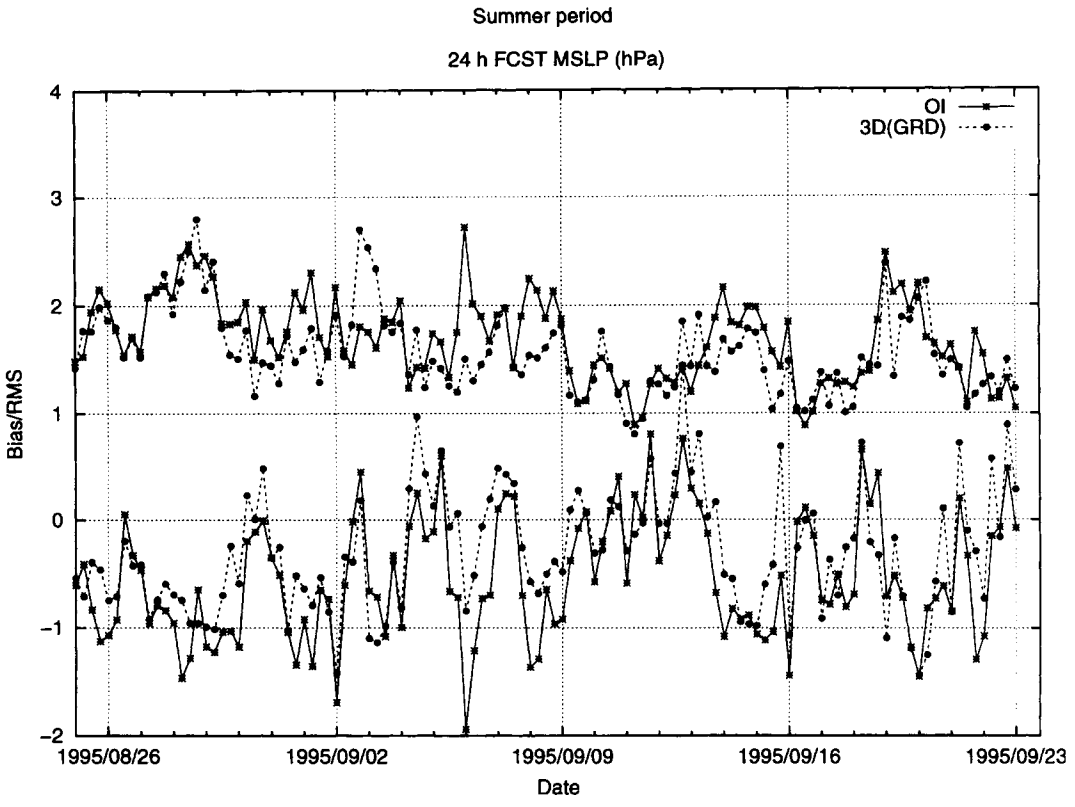

Fig. 3. Time variability of the +24 h P_{msl} forecast bias and rms scores (hPa) during the assimilation cycles of the summer period (25 August–24 September 1995). The scores are for OI (full) and 3D-Var with grid point forecast model (dashed with dots).

are rather similar, except for the 500 hPa level, where the spectral model forecasts are more biased.

4.2. *Winter period observation verification results*

Fig. 5 shows the time-averaged winter period bias and rms scores for the P_{msl} analyses and forecasts and T_{2m} forecasts, in comparison to the observations. The 3D-Var based P_{msl} forecasts using the spectral forecast model are less biased than the OI and 3D-Var forecasts using the grid point forecast model. The OI based forecasts of T_{2m} are more biased than the 3D-Var based forecasts. Better performance of forecasts launched from 3D-Var analyses, as compared to the forecasts launched from OI analyses, are clearly seen in terms of the rms scores. The rms scores of the forecasts started from 3D-Var analyses are relatively independent on whether a grid point or a spectral forecast model is used. As was the case for the summer period, a large temporal variability in observation verification scores is evident for the winter period (figures not shown).

Fig. 6 illustrates the time-averaged bias and rms scores for winter period analyses and forecasts of geopotential heights, temperatures and wind speeds at the 850, 500 and 300 hPa levels. The OI and 3D-Var wind forecasts are relatively unbiased, at all vertical levels. The 3D-Var spectral forecasts of 850 and 500 hPa temperatures, as well as of 500 and 300 hPa geopotential heights are less biased than the corresponding OI and 3D-Var grid point forecasts. On the other hand the 3D-Var spectral forecasts of 850 hPa geopotential heights are more biased than the corresponding OI and 3D-Var grid point forecasts. In terms of rms, the 3D-Var scores are seen to be clearly better for all

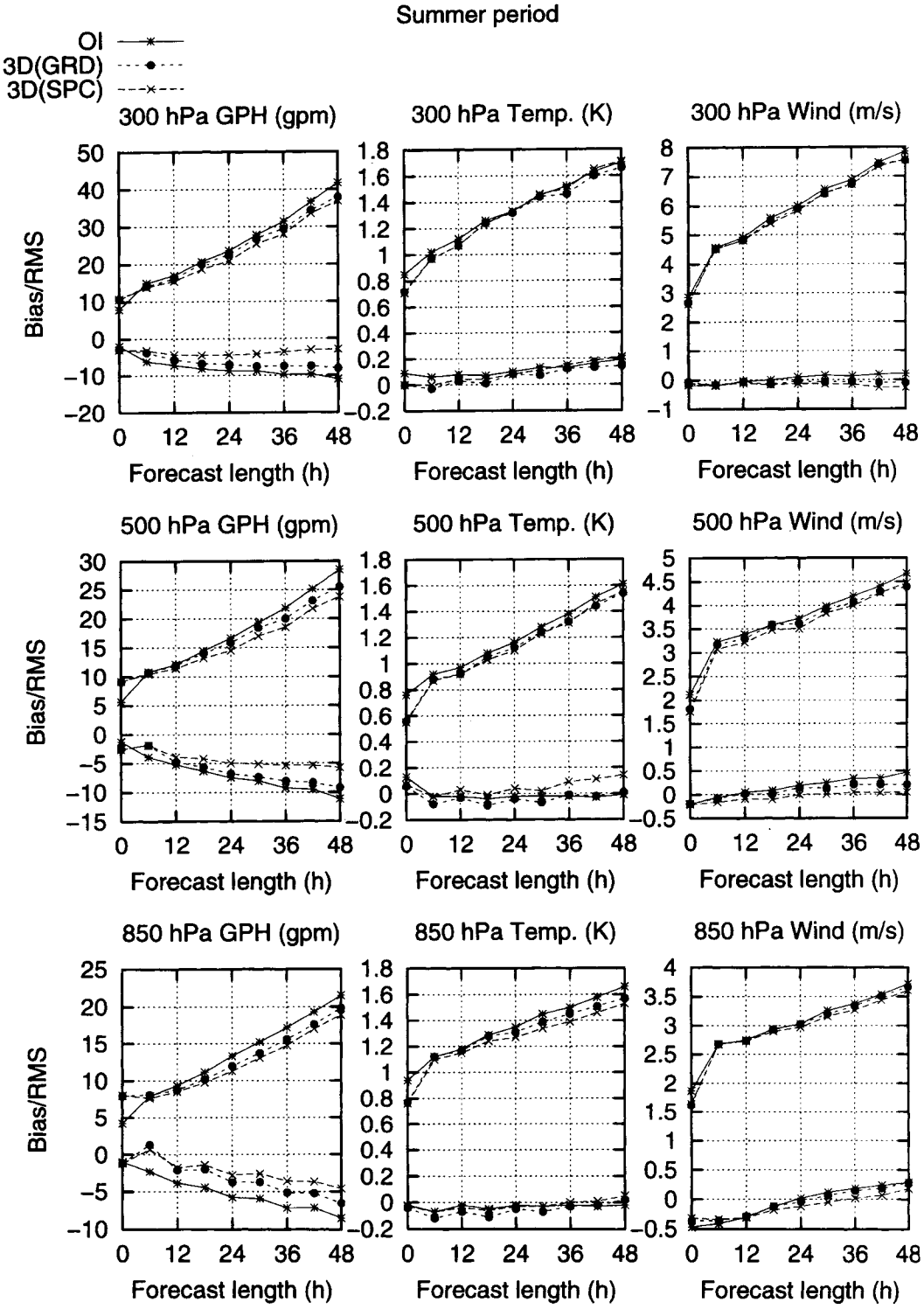

Fig. 4. Average bias and rms scores for summer period (25 August-24 September 1995) forecasts, at 300 hPa (upper), 500 hPa (middle) and 850 hPa (lower), as functions of forecast length (h). Left column shows geopotential height scores (gpm), middle column temperature scores (K) and right column wind speed scores (m/s). The scores are for OI (full), 3D-Var with grid point forecast model (dashed with dots) and 3D-Var with spectral forecast model (dashed with crosses).

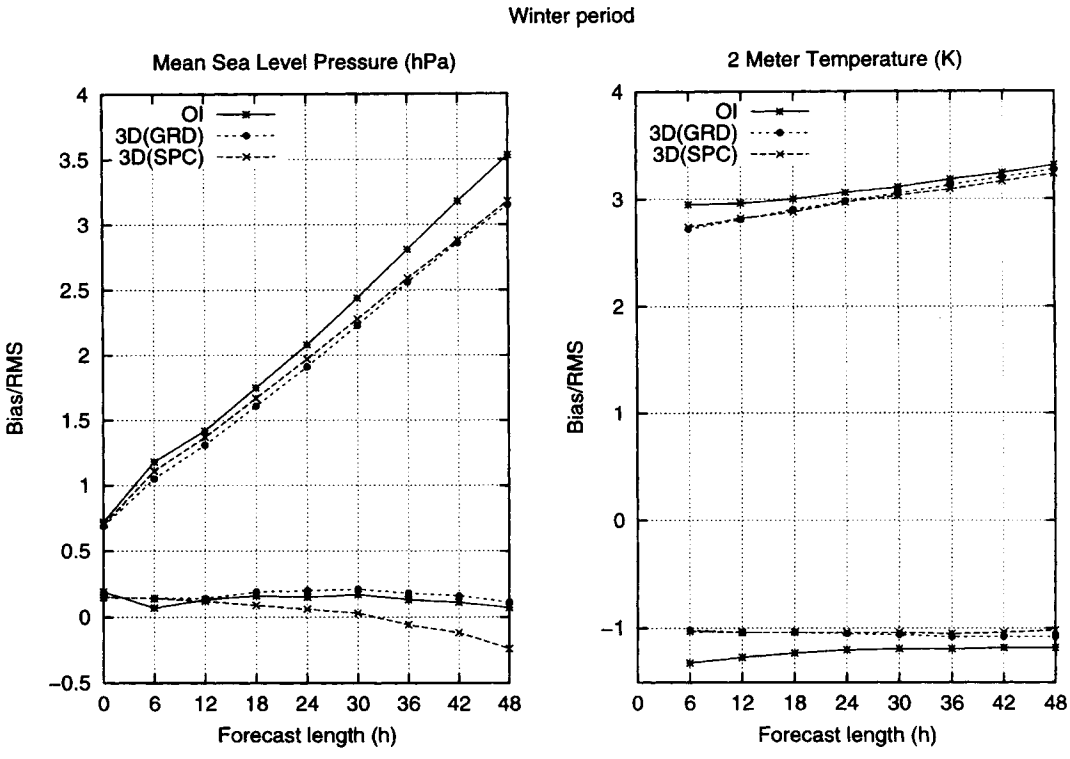

Fig. 5. Average bias and rms scores for winter period (10 February–9 March 1998) P_{msl} (left) and T_{2m} (right) forecasts as functions of forecast length (h). The P_{msl} (hPa) and T_{2m} (m/s) scores are for OI (full), 3D-Var with grid point forecast model (dashed with dots) and 3D-Var with spectral forecast model (dashed with crosses).

variables and vertical levels. The 3D-Var forecast rms scores are relatively independent of whether a grid point or spectral model has been used.

4.3. Case study and verification against analyses

Observation verification gives just one measure of the forecast quality. As most observations used in the verification package are located over continental Europe, the conclusions drawn from the observation verification are only valid over land. Even in the area where observations are dense and the observation verification scores are useful, analysis verification (using analyses to verify forecasts) and subjective verification may still be useful. To give an idea of how much difference in the forecasts one can expect from a large difference in the observation verification score, two cases are selected on the basis of Fig. 3. For the first case, started from 2 September 1995 18 UTC, the OI based +24 h P_{msl} forecast has a much smaller rms observation verification score than the 3D-Var based grid point model forecast. For the second case, started at 6 September 1995 00 UTC, the 3D-Var based +24 h grid point model forecast have much smaller rms observation verification score.

In Fig. 7, the two P_{msl} forecasts (middle) look rather similar to each other. Comparing the forecasts with the verifying analyses (upper), we may conclude that the OI and 3D-Var systems both failed to predict the position and the depth of the low. The depth of the low is somewhat better in the 3D-Var forecast while the position is slightly better in the OI forecast. Over continental Europe, the ridge is predicted better by the OI system. To quantify this comparison, the difference maps between forecasts and verifying analyses are shown at the bottom of the figure. From these two difference maps, our subjective evaluations are confirmed. The better observation verification score for this OI forecast is due to the slightly

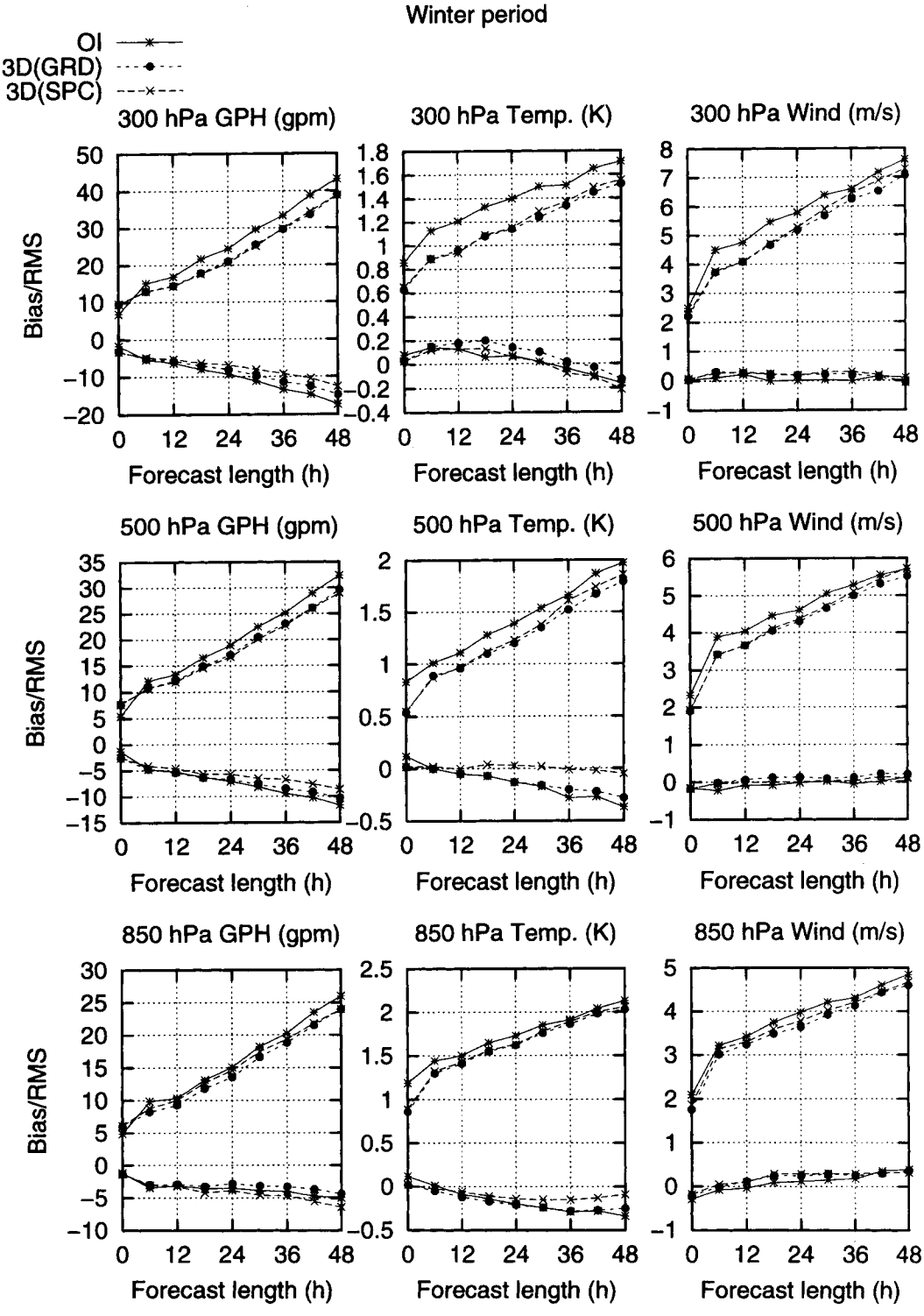

Fig. 6. Average bias and rms scores for winter period (10 February–9 March 1998) forecasts, at 300 hPa (upper), 500 hPa (middle) and 850 hPa (lower), as functions of forecast length (h). Left column shows geopotential height scores (gpm), middle column temperature scores (K) and right column wind speed scores (m/s). The scores are for OI (full), 3D-Var with grid point forecast model (dashed with dots) and 3D-Var with spectral forecast model (dashed with crosses).

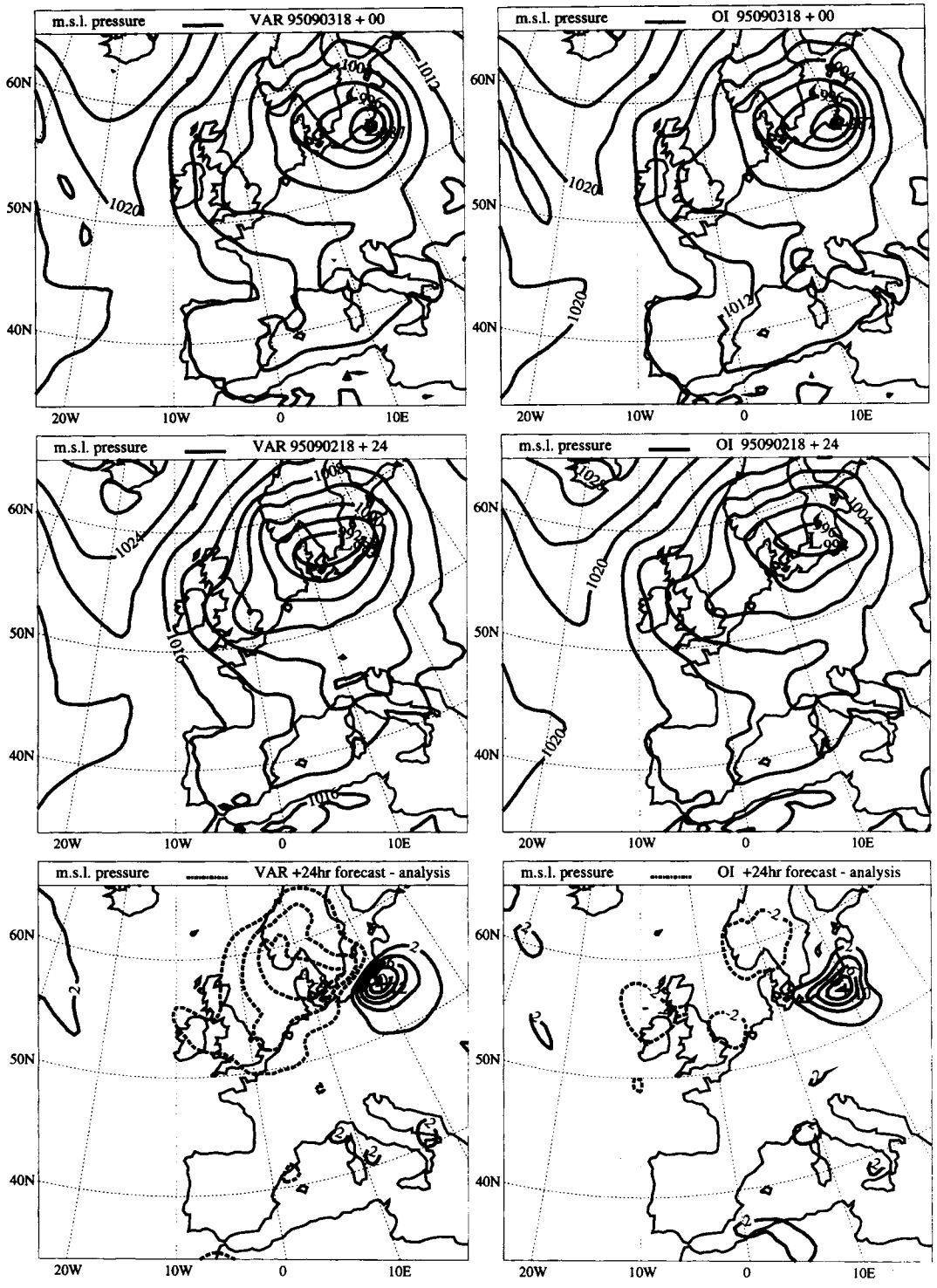

Fig. 7. Forecasts at 24 h (middle) of P_{msl}, valid on 3 September 1995 at 18 UTC, and corresponding verification analyses (upper). The contour interval is 4 hPa. Also shown (lower) are the differences between the +24 h P_{msl} forecasts and their corresponding verification analyses. The contour interval for the difference plots is 2 hPa and the zero-lines are suppressed. The results are for 3D-Var with grid point forecast model (left) and OI (right).

better position of the low and an almost error-free forecast over continental Europe, where we have the most dense synoptic verification observations.

In Fig. 8, the two P_{msl} forecasts (middle) also look rather similar to each other. However, the central pressures of the low differ by 3 hPa and the positions of the low center differ by 100 km. Comparing the forecasts (middle) with the verifying analyses (upper), the 3D-Var forecast for the low looks clearly better than the OI forecast. The difference maps (lower) also show that the errors of the 3D-Var forecast are significantly smaller. In the observation-dense area, this is especially true, which explains the large difference in the observation verification scores.

5. The effects of using all significant level data

One potential advantage of the HIRLAM 3D-Var, as compared to OI, is the use of all significant level data from TEMP and PILOT observation reports, rather than only standard level data. The standard pressure levels of TEMP reports are: 1000, 925, 850, 700, 500, 400, 300, 250, 200, 150, 100, 70, 50, 30, 20 and 10 hPa. The standard pressure levels of PILOT pressure level reports are: 850, 700, 500, 400, 300, 250, 200, 150, 100, 70, 50, 30, 20 and 10 hPa. To investigate the effects of using all significant level data the reference 3D-Var spectral run was complemented with a modified 3D-Var for the first week of the winter period experiment (10–16 February 1998). In the modified spectral run only standard pressure level data from TEMP reports and PILOT pressure level reports were assimilated.

The time averaged bias and rms scores for the 3D-Var reference and modified spectral runs are illustrated in Fig. 9 for the 700 and 200 hPa temperature and wind analyses and forecasts, in comparison to observations in the EWGLAM list. At 700 hPa, the differences in bias of the reference and modified forecasts are small. The magnitude of the bias is also small, both for temperatures and wind speeds. On the other hand, the bias of the 200 hPa temperatures and wind speeds are relatively large. The 200 hPa temperatures are positively biased and the 200 hPa wind speeds show a negative bias. The magnitude of the bias of the modified run is larger than for the reference run. The rms scores of the reference forecasts are in general slightly better for the 700 and 200 hPa temperatures, as compared to the scores of the modified run. It seems that the use of all significant level TEMP and PILOT pressure level data has a positive impact on the 3D-Var based forecasts.

6. Investigation of observation screening and variational quality control

To demonstrate the effects of the screening and the variational quality control (VarQC), the same randomly chosen assimilation cycle (5 March 1998 12 UTC) as is diagnosed in the companion paper by Gustafsson et al. (2001) is investigated. For this assimilation cycle the 3D-Var analysis system was also run without VarQC.

Since the effects of observation screening and VarQC are rather similar for the 3D-Var analyses utilising the spectral and the grid point forecast models, only results from the version with the spectral model are shown. To highlight the effects of VarQC the minimisations were performed until the quadratic norm of the cost function gradient had decreased by a factor 100, as compared to its initial value.

Table 3 illustrates the number of observed quantities of each observation type that are presented to the screening first guess check and the VarQC. In the 3D-Var 165 TEMP and 15 PILOT profiles are used. The table also shows the number of quantities rejected by the respective quality control algorithms and the rejection ratio, i.e., the fraction (in %) of the total number of observed quantities that are rejected in either the first guess check or the VarQC. Here we consider an observation to be rejected by the VarQC if the weight given to the observation in the analysis has been reduced by a factor of 0.25 or more. The number of observed quantities of each observation type that are presented to the OI first guess and the OI check are shown in Table 4, together with the number of quantities rejected by the respective quality control algorithms and the rejection ratios. The OI check is the spatial consistency check in the OI (Lorenc, 1981) that corresponds to the VarQC. In the OI 166 TEMP and 23 PILOT profiles were used.

The main difference between the VarQC and the OI check is that all observations are used to

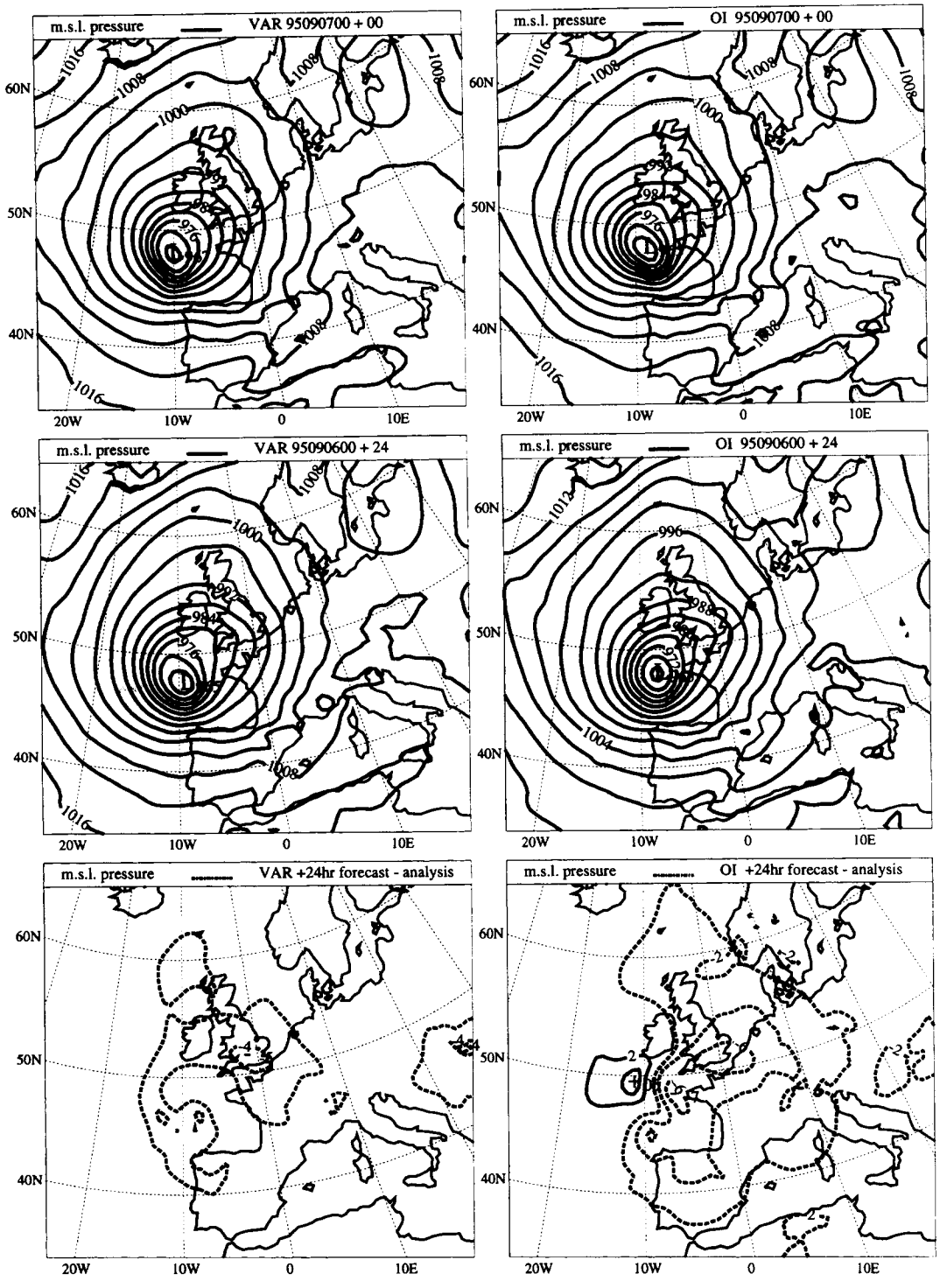

Fig. 8. Forecasts at 24 h (middle) of P_{msl}, valid on 7 September 1995 at 00 UTC, and corresponding verification analyses (upper). The contour interval is 4 hPa. Also shown (lower) are the differences between the +24 h P_{msl} forecasts and their corresponding verification analyses. The contour interval for the difference plots is 2 hPa and the zero-lines are supressed. The results are for 3D-Var with grid point forecast model (left) and OI (right).

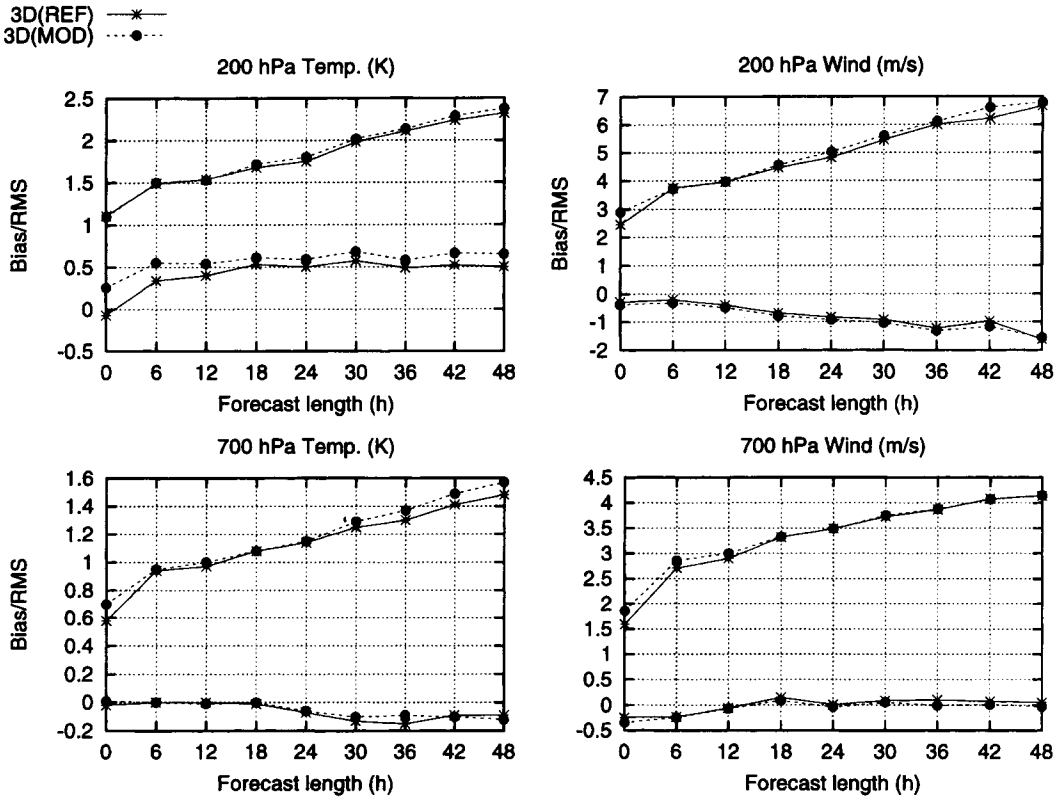

Fig. 9. Average bias and rms scores for the first week of the winter period (10–16 February 1998), as functions of forecast length (h). Temperature scores (K) at 700 hPa (lower left) and 200 hPa (upper left) as well as wind speed scores (m/s) at 700 hPa (lower right) and 200 hPa (upper right). The scores are for the reference spectral 3D-Var run (full) with all significant level data used and for the modified run (dashed) with only standard pressure level data from TEMP and PILOT pressure level reports used.

Table 3. *3D-Var data usage and rejections for the analysis valid for 5 March 1998 12 UTC; the analysis made use of 165 TEMP and 15 PILOT profiles*

Observation type	Observed quantity	Obs. before FG and VarQC	Obs. rejected in FG check	Obs. rejected in VarQC	Rejection ratio (%)
SYNOP	geopotential	2032	4	93	4.8
SHIP	geopotential	221	0	5	2.3
	10 m wind	217	2	4	2.8
DRIBU	geopotential	58	0	0	0.0
AIREP	temperature	1137	9	4	1.1
	wind	1134	10	30	3.5
PILOT	wind	114	0	2	1.8
TEMP	temperature	5877	269	32	5.1
	wind	5224	51	151	3.9
	spec. hum.	4380	168	2	3.9

Table 4. *OI data usage and rejections for the analysis valid for 5 March 1998 12 UTC; the analysis made use of 166 TEMP and 23 PILOT profiles*

Observation type	Observed quantity	Obs. before FG and OI check	Obs. rejected in FG check	Obs. rejected in OI check	Rejection ratio (%)
SYNOP	geopotential	2024	39	11	2.5
	10 m wind	963	15	1	1.7
SHIP	geopotential	238	3	7	4.2
	10 m wind	238	1	7	3.4
DRIBU	geopotential	59	2	0	3.4
	wind	14	0	0	0.0
AIREP	wind	1135	17	5	1.9
PILOT	wind	80	0	0	0.0
TEMP	geopotential	2083	83	2	4.1
	wind	1962	3	3	0.3
	rel. hum.	938	29	12	4.4

support or reject an observation in the VarQC, due to the global data usage in 3D-Var, while the OI check only uses nearby observations. Furthermore, at present there is no direct dependence in VarQC on the first guess or analysis error standard deviations, as in the OI check. Thus, the OI check is less stringent over data-sparse areas, where the analysis error standard deviations are larger than over well observed regions. Finally, due to the iterative nature of the variational minimisation procedure, observations are not definitively rejected or accepted at a fixed calculation step (until iteration 70) in VarQC, which is the case with the OI check.

By comparing Table 3 with Table 4 the larger amount of data from PILOT and TEMP reports used in 3D-Var is evident. This is due to the use of all significant level data in 3D-Var. The number of rejections of an observed quantity in each of the two types of checks in general differs substantially between the OI and the 3D-Var systems. However, the rejection ratios seem realistic and are of the same order of magnitude for both assimilation systems and for all quantities.

The effects of the VarQC rejections, in the case of surface pressure, are illustrated by Fig. 10. The upper part shows the surface pressure analysis increments for a 3D-Var analysis when VarQC is not applied. The lower part shows the difference in analysed surface pressure between the analysis when VarQC is not applied and the analysis when VarQC is applied. From the lower part, the positions of rejected observations may be identified and in combination with the upper part it can be seen that the effects of VarQC on the analysis are most evident due to rejection of the observations located over Northern Atlantic, North Africa and Western Russia, respectively. Table 3 illustrates that 93 land surface geopotential observations and 5 sea surface geopotential observations are rejected due to VarQC. On the other hand, from the lower part of Fig. 10. it can be seen that large differences appear mainly over less than 15 geographical locations.

Fig. 11 shows the cost function as a function of the number of cost function evaluations, for a minimisation when VarQC is not applied and for a minimisation when VarQC is applied. It can be seen that the cost functions start to deviate after 20 iterations, when VarQC is switched on and reduces the contribution to the cost function from some observations. The rapid decrease of the cost function at evaluation 75, for the minimisation when VarQC is applied, is due to the fact that observations rejected in VarQC are now completely removed from the minimisation so that the problem becomes completely quadratic.

7. Discussion and concluding remarks

A 3-dimensional variational data assimilation for HIRLAM has been developed. It has been given an incremental formulation for computation economy reasons and to permit application together with the spectral as well as the grid point HIRLAM models. The general formulation of the HIRLAM 3D-Var is described in a companion

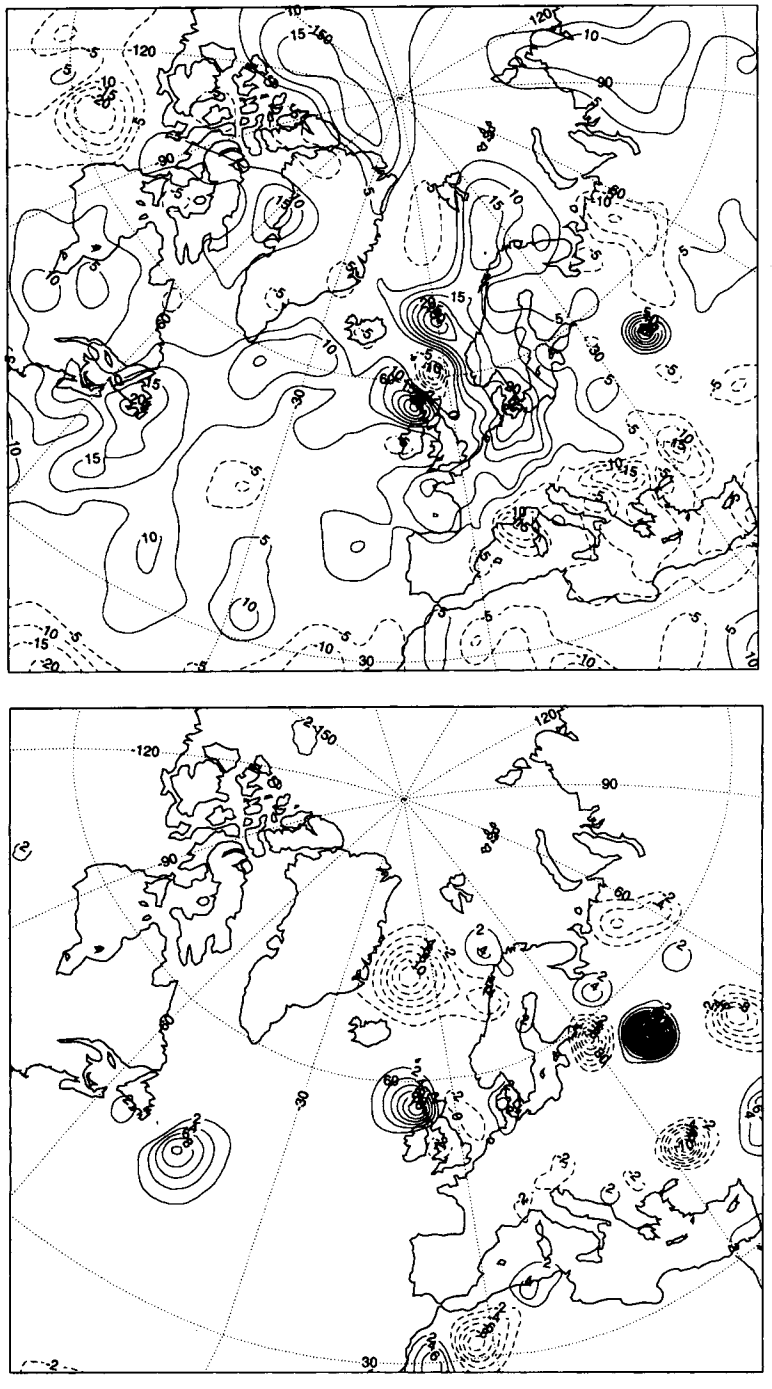

Fig. 10. Surface pressure analysis increments (upper), in tenths of hPa, for 3D-Var with spectral forecast model and with VarQC not applied. Surface pressure analysis difference (lower), in tenths of hPa, between one 3D-Var analysis with VarQC not applied and one with VarQC applied. The analyses are valid for 5 March 1998 12 UTC and the contour interval for the upper and lower maps are 0.5 and 0.2 hPa, respectively.

paper (Gustafsson et al., 2001). The 3D-Var system includes an observation handling system, that is designed to work efficiently on different kinds of computer architectures and to meet future requirements regarding the increasing amount of observations and assimilation of new data types.

Results of two sets of data assimilation experiments indicate that the 3D-Var analysis system performs significantly better than the HIRLAM systems based on statistical interpolation.

The observation handling is believed to be one major contributing factor to the superiority of the 3D-Var scheme. One advantage of the HIRLAM 3D-Var, as compared to the OI system, that has been demonstrated, is the use of all significant level data from multilevel observation reports. Other attractive features are the use of variational quality control, which accounts for non-Gaussian observation errors, and the elimination of data selection. With regard to the background error constraint, which is described in the companion paper by Gustafsson et al. (2001), an important advantage of the 3D-Var is the use of non-separable structure functions.

The 3D-Var system has been proven to outperform the OI system, regardless of whether it is used together with the spectral or the grid point HIRLAM models. The summer case indicated better forecast verification scores for the 3D-Var based spectral model forecasts, as compared to the grid point model forecasts, while the winter case experiment indicated less conclusive verification scores in this respect. It is not clear whether the improved summer time forecasts with the spectral model are related to an improved numerical accuracy of the spectral model, as compared to the grid point model. Another reason may be a degrading effect of adding a lower resolution increment, defined in spectral space, to a full resolution background field in grid point space, in case of using 3D-Var together with the grid point model.

Further improvements regarding observation handling include assimilation of new data types, such as the Global Positioning System (GPS) total

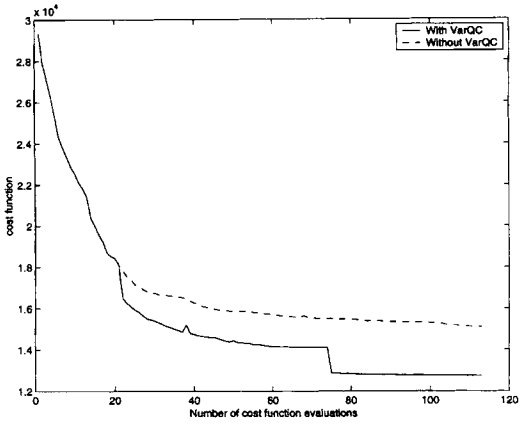

Fig. 11. Evolution of cost function for an analysis with VarQC not applied (dashed line) and with VarQC applied (full line) as a function of the number of cost function evaluations.

atmospheric delays, radar radial winds (Lindskog et al., 2000) and satellite radiances. The future introduction of 4-dimensional variational data assimilation (4D-Var), which is the natural extension of 3D-Var, will lead to an observation handling that is more consistent in the time dimension.

8. Acknowledgements

The development of the HIRLAM observation handling system has greatly benefited from co-operation with, and advice from, the ECMWF data assimilation staff. Without any particular order of preference, we would like especially to thank Erik Andersson, Heikki Järvinen, Sami Saarinen, Per Undén and Drasko Vasiljević. We also thank the anonymous reviewers for useful comments.

The development of the HIRLAM 3D-Var was partly carried out with support from the European Commission's programme Environment and Climate (Project NEWBALTIC II, Contract No. ENV4-CT97-0626) and with support for assimilation of ground-based GPS data from the Swedish National Space Board (Contract DNr 153/98 SSF).

REFERENCES

Andersson, E. and Järvinen, H. 1999. Variational quality control. *Q. J. R. Meteorol. Soc.* **125**, 697–722.

Bergthorsson, P. and Döös, B. 1955. Numerical weather map analysis. *Tellus* **7**, 329–340.

Courtier, P., Andersson, E., Heckley, W., Pailleux, J., Vasiljević, D., Hamrud, M., Hollingsworth, A., Rabier, F. and Fisher, M. 1998. The ECMWF implementation of three dimensional variational assimilation (3D-Var). Part I: Formulation. *Q. J. R. Meteorol. Soc.* **124**, 1783–1808.

Geleyn, J.-F. 1988. Interpolation of wind, temperature and humidity values from the model levels to the height of measurement. *Tellus* **40**, 347–351.

Gustafsson, N. 1999. The numerical scheme and lateral boundary conditions for the spectral HIRLAM and its adjoint. *ECMWF Seminar Proceedings.* Recent developments in numerical methods for atmospheric modelling, ECMWF, Reading, UK, 7–11 September 1998, 335–363.

Gustafsson, N., Lönnberg, P. and Pailleux, J. 1997. Data assimilation for high resolution limited area models. *J. Met. Soc. of Japan* **75**, 367–382.

Gustafsson, N., Berre, L., Hörnquist, S., Huang, X.-Y., Lindskog, M., Navascués, B., Mogensen, K. S. and Thorsteinsson, S. 2001. Three-dimensional variational data assimilation for a limited area model. Part I: General formulation and the background error constraint. *Tellus* **53A**, this issue.

Holtslag, A. A. M. and Bovine, B. A. 1993. Local versus nonlocal boundary-layer diffusion in a global climate model. *J. Clim.* **6**, 1825–1842.

Ingleby N. B. and Lorenc, A. C. 1993. Bayesian quality control using multivariate normal distibutions. *Q. J. R. Meteorol. Soc.* **119**, 1195–1225.

Lindskog, M., Järvinen, H. and Michelson, D. B. 2000. Assimilation of radar radial winds in the HIRLAM 3D-Var. *Phys. Chem. Earth (B)* **25**, 1243–1249.

Lorenc, A. 1981. A global three-dimensional multivariate statistical interpolation scheme. *Mon. Wea. Rev.* **109**, 701–721.

Lorenc, A. 1986. Analysis methods for numerical weather prediction. *Q. J. R. Meteor. Soc.* **112**, 1177–1194.

Lorenc, A. and Hammon, O. 1988. Objective quality control of observations using Bayesian methods. Theory and practical implementation. *Q. J. R. Meteorol. Soc.* **114**, 515–543.

Louis, J. F. 1979. A parametric model of vertical eddy fluxes in the atmosphere. *Bound.-Layer Meteorol.* **17**, 187–202.

Machenhauer, B. 1977. On the dynamics of gravity oscillations in a shallow water model, with application to normal mode initialization. *Beitr. Phys. Atmos.* **50**, 253–271.

Parrett, C. A. 1992. Background errors for the quality control and assimilation of atmospheric observations in the unified model — the situation in July 1992. In: *UK Met. Office Short Range Forecasing Reaearch Technical Report* **22**, July 1992, 22 pp.

Parrish, D. F. and Derber, J. C. 1992. The National Meteorological Centre's spectral statistical interpolation analysis system. *Mon. Wea. Rev.* **120**, 1747–1763.

Rantakokko, J. 1997. Strategies for parallel variational data assimilation. *Parallel Computing* **23**, 2017–2039.

Sass, B. H., Nielsen, N. W., Jørgensen, J. U. and Amstrup, B. 1999. The operational HIRLAM system at DMI. *DMI Tech. Rep.* no. **99–21**, 42 pp, October 1999. Available from DMI, Lyngbyvej 100, Copenhagen.

Savijärvi, H. 1989. Fast radiation parameterization schemes for mesoscale and short-range forecast models. *J. Appl. Meteor.* **29**, 437–447.

Sundqvist H., Berge, E. and Kristjansson, J. E. 1989. Condensation and cloud parameterization studies with a mesoscale numerical weather prediction model. *Mon. Wea. Rev.* **117**, 1641–1657.

Sundqvist, H. 1993. Inclusion of ice phase of hydrometeors in cloud parameterization for mesoscale and large scale models. *Beitr. Phys. Atmosph.* **66**, 137–147.